

# Machine Learning-Assisted Thermoelectric Cooling for On-Demand Multi-Hotspot Thermal Management

Jiajian Luo<sup>1</sup> and Jaeho Lee<sup>1,a)</sup>

<sup>1</sup>*Department of Mechanical and Aerospace Engineering, University of California Irvine, Irvine, CA, 92697, USA*

The rapid emergence of System-on-Chip (SoC) technology introduces multiple dynamic hotspots with spatial and temporal evolution to the system, necessitating a more efficient, sophisticated, and intelligent approach to achieve on-demand thermal management. In this study, we present a novel machine learning-assisted optimization algorithm for thermoelectric coolers (TECs) that can achieve global optimal temperature by individually controlling TEC units based on real-time multi-hotspot conditions across the entire domain. A convolutional neural network (CNN) with inception module is trained to comprehend the coupled thermal-electrical physics underlying the system and attain accurate temperature predictions with and without TECs. Due to the intricate interaction among passive thermal gradient, Peltier effect and Joule effect, a local optimal TEC control experiences spatial temperature trade-off which may not lead to a global optimal solution. To address this issue, a backtracking-based optimization algorithm is developed using the designed machine learning model to iterate all possible TEC assignments for attaining global optimal solutions. For any  $m \times n$  matrix with  $N_{\text{HS}}$  hotspots ( $n, m \leq 10, 1 \leq N_{\text{HS}} \leq 20$ ), our algorithm is capable of providing global optimal temperature and its corresponding TEC array control in an average of 1.07 second while iterating through tens of temperature predictions behind-the-scenes. This represents a speed increase of over four orders of magnitude compared to traditional FEM strategies which take approximately 18 minutes.

## I. INTRODUCTION

Despite great advancements in semiconductor technology beyond the sub-3nm node <sup>1</sup>, most thermal management techniques nowadays are limited to the macroscale operation. The trend towards device miniaturization and the rapid emergence of System-on-Chip (SoC) inevitably complicate the thermal behavior within microelectronic devices <sup>2,3</sup>. Specifically, multiple on-chip hotspots exhibit spatial and temporal changes due to workload variations, environmental fluctuations, device defects and aging, which can occur among modules <sup>4,5</sup>, cores (processors) <sup>6,7</sup> and transistors <sup>8</sup>. The complexity of the hotspot behavior presents unprecedented challenges for conventional thermal management methods which only rely on uniform control, necessitating a more efficient, sophisticated, and intelligent approach capable of on-demand thermal management to ensure optimal functionality and longevity of microelectronic devices <sup>9</sup>.

Among various active cooling techniques, thermoelectric coolers (TECs) offer distinctive local cooling capability as well as several other advantages<sup>10-12</sup>, making them a promising solution to hotspot thermal management. In recent years, there have been emerging designs utilizing single TECs <sup>13-16</sup> and TEC arrays <sup>17-19</sup> for on-chip hotspot cooling in microelectronic devices. However, TEC cooling exhibits significant spatial temperature trade-offs due to heat redistribution, and its performance relies on multiple variables including TEC voltage and hotspot conditions<sup>12,20</sup>. The high non-linearity in TEC behavior requires

---

<sup>a)</sup> Correspondence author. Email: jaeholee@uci.edu.

multiple solutions for optimization, which brings expensive computational cost to conventional finite element method (FEM) simulations. Furthermore, in actual applications where multiple hotspots undergo spatial and temporal evolution, the original technique becomes more challenging and even impossible to realize a real-time optimal TEC control.

The thriving field of machine learning offers a powerful tool for thermoelectric research by providing neural network models that greatly expedite the process of thermoelectric material selection<sup>21</sup>, TEC modelling<sup>22</sup> and optimization<sup>23,24</sup>. However, these models primarily focus on the analysis of back-end designs by considering an individual, isolated TEC device<sup>21,22</sup>, or using over-simplified optimization logics such as uniform control<sup>23</sup> or linear control<sup>24</sup>. Apparently, there is still vacancy and urgent need for a more comprehensive model that can comprehend the coupled thermal-electrical physics in TECs while predicting their spatial interplays with multiple hotspots undergoing dynamic evolution across the entire domain. Ultimately, this model should be capable of providing responsive TEC control over the entire domain to achieve real-time global optimal temperature.

In this study, we present a machine learning-assisted optimization algorithm for thermoelectric cooling that fulfills the aforementioned on-demand thermal management. We utilize our previous holey silicon-based TEC array with independent TEC control<sup>25</sup> as an illustrative example for conducting the analysis. We develop a convolutional neural network (CNN) with inception module to perceive the spatial correlation of TECs and hotspots, thereby accurately predicting temperatures by comprehending the thermal-electrical physics underlying the system. During the TEC optimization process, the major difficulty lies in the intricate thermal-electrical interaction among multiple hotspots and TECs, since a local optimal TEC control may not lead to a global optimal solution due to temperature redistribution. Therefore, we develop a backtracking-based optimization algorithm that efficiently explores all potential TEC assignments in order to obtain the global optimal temperature based on real-time hotspot conditions. Note that this methodology can be applied to general TEC / TEC array designs with a wide range of thermoelectric materials (e.g.,  $\text{Bi}_2\text{Te}_3/\text{Sb}_2\text{Te}_3$ ), configurations (e.g., lateral- and vertical-oriented TECs) and device scales (e.g., module-scale and transistor-scale). Consequently, this approach can hopefully provide efficient TEC/ TEC array control logic for the future TEC-incorporated microelectronic systems.

## II. TEC MODELLING

To demonstrate our study, we choose our previous theoretical designs<sup>25</sup>, the holey silicon-based single TEC (Fig. 1a) and its scaling array (Fig.1b) as our TEC model. The model features a lateral orientation of the TEC components (i.e., Peltier electrodes and holey silicon region) along with the central hotspot. Here, holey silicon is the thermoelectric material due to its

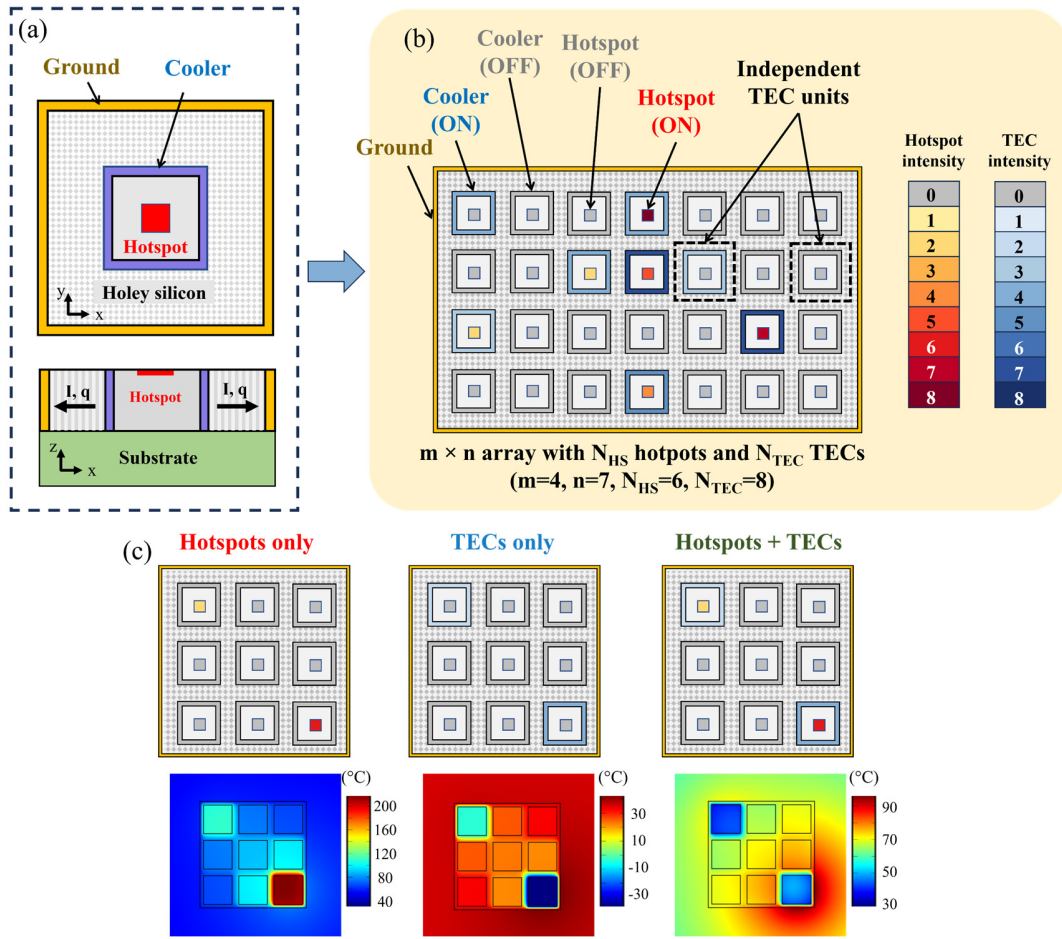


FIG. 1. Holey silicon-based lateral TEC and its array model. (a) Schematics of a single TEC. (b) Schematics of an arbitrary  $m \times n$  TEC array with  $N_{HS}$  assigned hotspots and  $N_{TEC}$  assigned TECs ( $1 \leq m, n \leq 10$ ;  $0 \leq N_{HS}, N_{TEC} \leq \min[m \times n, 20]$ ). The intensity of hotspots and TECs are in 9 discrete levels. (c) FEM modelling example of a  $3 \times 3$  hotspot-TEC array with three scenarios: hotspots only, TECs only and hotspots + TECs.

compatibility with microfabrication processes, and because the introduction of vertical nanoholes results in substantial decrease of in-plane thermal conductivity due to phonon boundary scattering, meanwhile retaining excellent electrical properties (electrical conductivity and Seebeck coefficient) from p-type silicon<sup>26-29</sup>. When positive voltage is applied to the cooler, lateral heat redistribution occurs which provides active heat removal from the hotspot to the in-plane surroundings. Compared to a single TEC, the TEC array as shown in Fig. 1b has multiple coolers enclosed by a single ground that allow for independent TEC control. Based on the existing hotspot conditions, different coolers can accept different input voltages to achieve on-demand thermal management.

In general, the TEC modelling involves thermal-electrical physics which includes passive heat diffusion, thermoelectric effect and Joule effect. In steady state, the governing equations can be written as:

$$\nabla \cdot \mathbf{q} = Q_e \quad (1)$$

$$Q_e = \mathbf{J} \cdot \mathbf{E} \quad (2)$$

$$\mathbf{q} = ST\mathbf{J} - k\nabla T \quad (3)$$

$$\mathbf{J} = -\sigma(\nabla V + S\nabla T) \quad (4)$$

where  $\mathbf{q}$  is heat flux vector,  $Q_e$  is Joule heat,  $\mathbf{J}$  is current density vector,  $\mathbf{E}$  is electric field vector,  $S$  is Seebeck coefficient,  $T$  is absolute temperature,  $k$  is thermal conductivity,  $V$  is voltage and  $\sigma$  is electrical conductivity. Eq. 1 and Eq. 2 represent heat transfer in a thermoelectric material, where Joule heating is considered as the primary source of internal heat generation. Eq. 3 defines the total heat flux which combines the Peltier effect and traditional heat conduction dictated by Fourier's law. Eq. 4 describes the current density as driven by both electric potential and temperature gradients as a result of the Seebeck effect. In our TEC model, the thermal conductivity, Seebeck coefficient and electrical conductivity of holey silicon are set at 1 W/mK, 450  $\mu\text{V/K}$  and  $5.4 \times 10^4$  S/m, respectively, representing a 30% porosity, 20 nm neck size and highly doped P-type holey silicon thin film at elevated temperature<sup>28,29</sup>. The ambient temperature is set at 30 °C and the array boundary is set to be laterally conducted. Considering the target in transistor-scale thermal management, the size of one cooler unit is defined at  $1 \times 1 \mu\text{m}^2$ . Besides, to investigate the scaling effect and provide more flexibility, the TEC array can have arbitrary  $m$  rows and  $n$  columns ( $1 \leq m, n \leq 10$ ) with random  $N_{\text{HS}}$  assigned hotspots and  $N_{\text{TEC}}$  assigned TECs ( $0 \leq N_{\text{HS}}, N_{\text{TEC}} \leq \min[m \times n, 20]$ ). To simplify the problem while exaggerating the temperature difference, the assigned hotspot heat flux and assigned TEC voltage are pre-defined with 8 discrete intensities, ranging from  $1 \times 10^{15}$  W/m<sup>3</sup> to  $8 \times 10^{15}$  W/m<sup>3</sup> (an interval of  $1 \times 10^{15}$  W/m<sup>3</sup>) and from 25mV to 200mV (an interval of 25mV), respectively. Fig. 1c demonstrates a specific example of using 2D steady-state FEM simulations for a  $3 \times 3$  TEC array. From the simulations, a temperature map can be numerically derived given the values of  $m$ ,  $n$ ,  $N_{\text{HS}}$ ,  $N_{\text{TEC}}$  and their corresponding intensity levels.

### III. NEURAL NETWORK DEVELOPMENT

Fig. 2 illustrates the research workflow which includes massive data generation and data postprocessing. Here, we utilize MATLAB R2021a to generate random hotspot and TEC inputs based on the given constraints, which will be sequentially fed to COMSOL 6.0 to conduct FEM simulations and evaluate temperature maps as outputs. In MATLAB, the random values of rows ( $m$ ) and columns ( $n$ ) in the TEC array will be first defined. Later, two random  $m \times n$  matrixes with values from 0 to 8 will be generated, representing the hotspot and TEC levels. The maximum number of assigned hotspots ( $N_{\text{HS}}$ ) and TECs ( $N_{\text{TEC}}$ ) depend not only on the model constraints but also on the robustness of the training process. Here, we select  $\min[m \times n, 36]$  as the maximum number since it exceeds the original span ( $0 \leq N_{\text{HS}}, N_{\text{TEC}} \leq \min[m \times n, 20]$ ) for providing more robust predictions,

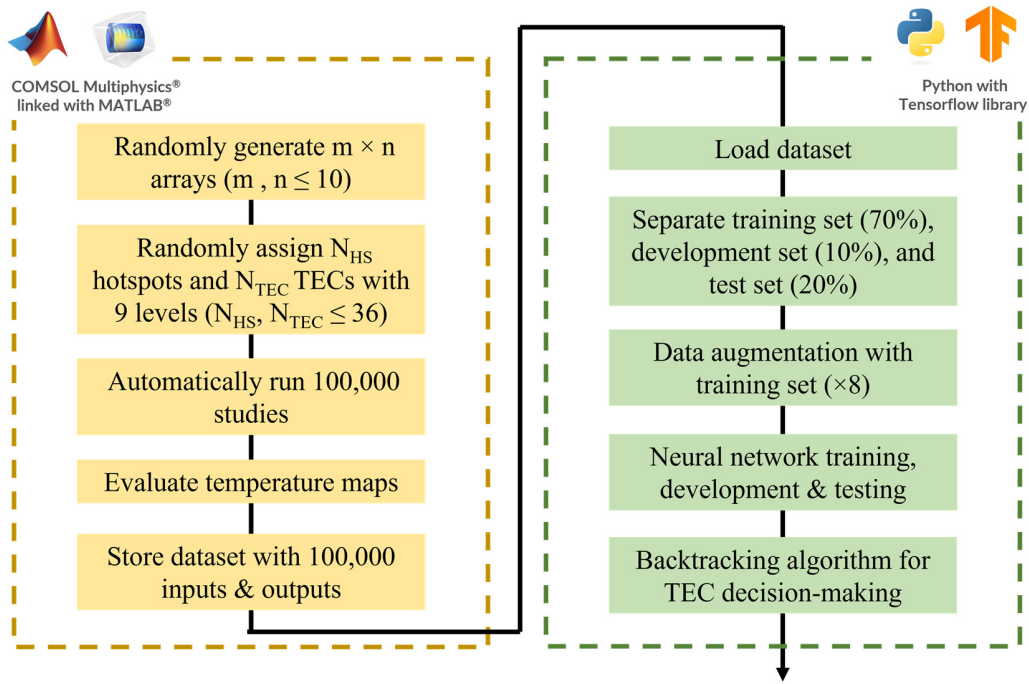


FIG. 2 Research workflow. (left) Massive data generation based on autonomous FEM simulations and (right) Data postprocessing, including data splitting, data augmentation, neural network training and TEC optimization algorithm design.

meanwhile, it is not so large to weaken the independency of individual units. With the defined hotspot and TEC inputs, steady-state FEM simulations will be conducted, followed by the evaluation of temperature maps. Eventually, the unit average temperature will be stored in an  $m \times n$  matrix as the corresponding output. The autonomous program continuously generates 100,000 random samples, whose total number considers the complexity of the model, the desired accuracy and the computation resources. After generating the original dataset, data splitting of training set (70%), development set (10%) and test set (20%) is performed. The training set is further augmented with the transformation of flipping (horizontal and vertical), rotation ( $90^\circ$ ,  $180^\circ$  and  $270^\circ$ ) and their combinations, resulting in a total number of training samples as 8 times as the original (560,000). This augmentation offers a cost-effective way to improve the model's accuracy and robustness [ref], thereby facilitating the learning of inherent symmetries in thermal-electrical physics.

Due to the necessity to generate a 2D temperature map and its significant relevance to the spatial correlation among hotspots and TECs, a convolutional neural network (CNN) is chosen as the base model<sup>30</sup>. However, most CNN models in literature, such as LeNet-5<sup>31</sup>, VGG16<sup>32</sup> and GoogLeNet<sup>33</sup>, are primarily designed for classification tasks. Therefore, modifications are necessary to adapt CNN models for regression tasks with continuous output values. After conducting multiple tests and comparison, we have developed a CNN model based on inception module<sup>33,34</sup> over other options (e.g., encoder-



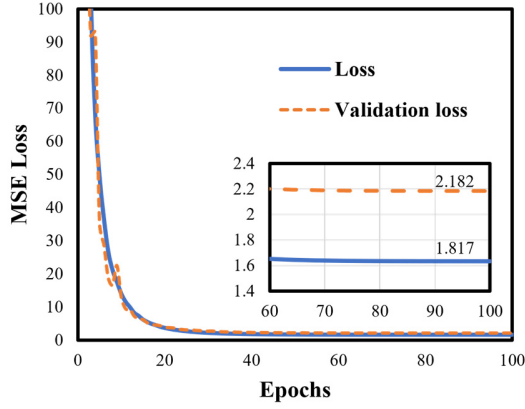


FIG. 4. MSE training loss as a function of training epochs

TABLE I. Summary of MSE loss.

Training Loss (70% data)	Validation Loss (10% data)	Test Loss (20% data)
1.817	2.182	1.252

$$\text{MSE} = \frac{1}{M \times N} \sum_i^M \sum_j^N (Y_{i,j} - \hat{Y}_{i,j})^2 \quad (5)$$

where  $Y_{i,j}$  is the ground-truth temperature in  $i^{\text{th}}$  row and  $j^{\text{th}}$  column,  $\hat{Y}_{i,j}$  is the predicted temperature in  $i^{\text{th}}$  row and  $j^{\text{th}}$  columns,  $M$  and  $N$  are the maximum numbers of rows and columns, respectively (i.e.,  $M = N = 10$ ). Fig. 4 demonstrate the MSE loss in the first 100 training epochs. With a learning rate of 0.001 and a batch size of 500 samples, the loss decreases rapidly through the first 40 epochs and stabilizes the third decimal through the 98<sup>th</sup> epoch. Table I summarizes the MSE loss for the training set, development set and test set.

While MSE is sensitive to large values and offers a smooth and differentiable function for the training, the mean absolute error (MAE)<sup>42</sup> provides a more interpretable evaluation of temperature prediction. The MAE loss is defined as:

$$\text{MAE} = \frac{1}{m \times n} \sum_i^m \sum_j^n |Y_{i,j} - \hat{Y}_{i,j}| \quad (6)$$

where  $m$  and  $n$  represent the actual number of rows and columns before padding, respectively. Fig. 5 demonstrates the analysis of MAE loss with additional 4200 samples, where 10 random samples are taken into average for every combination of x-axis and y-axis arguments. As shown in Fig. 5a, a relatively small and uniform MAE loss occurs when no TEC is assigned. However, when any TEC is assigned, the MAE loss becomes generally large and will be impacted by the array rows and columns. This is because the implementation of thermoelectric effect significantly increases the model complexity compared to a pure heat transfer model. It should be noted that the number of assigned TECs does not significantly impact the MAE loss when more than one TEC is assigned, as shown in Fig. 5d.

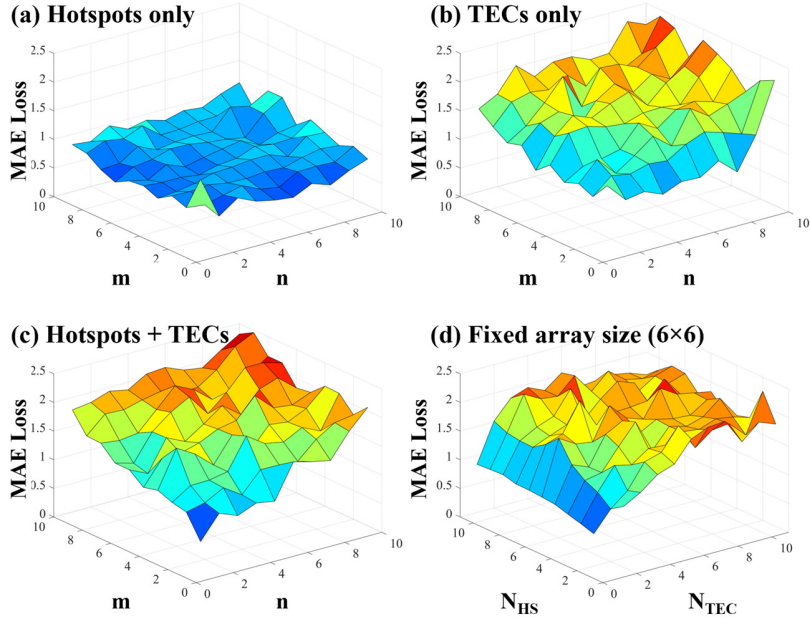


FIG. 5. Loss analysis of 4200 random samples. 10 random samples are taken into average for every combination of x-axis and y-axis variables. (a-c) MAE loss as a function of array dimensions ( $1 \leq m, n \leq 10$ ) in 3000 samples. (a) Hotspots only. (b) TECs only. (c) Hotspot + TEC. (d) MAE loss as a function of hotspot and TEC counts ( $1 \leq N_{HS}, N_{TEC} \leq 10$ ) in a  $6 \times 6$  TEC array in 1200 samples.

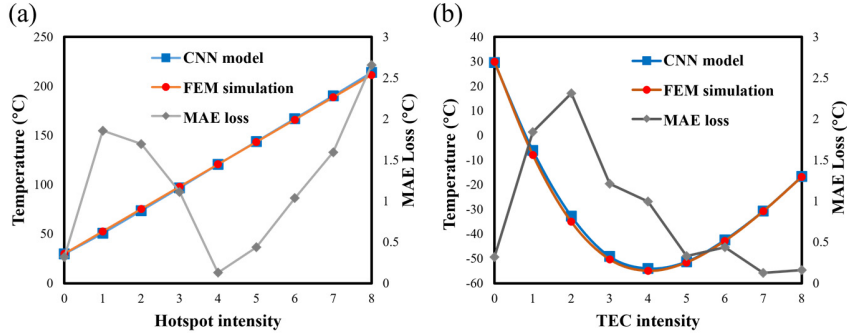


FIG. 6. Predictions of  $1 \times 1$  array. (a) Hotspot only. (b) TEC only.

The predictions of a  $1 \times 1$  TEC array (i.e., a single TEC) under hotspot only and TEC only scenarios are illustrated in Fig. 6. Among these predictions, the MAE loss can be simply interpreted as the temperature error in a single TEC. The results show that the CNN model not only captures the proportional relationship between temperature and hotspot intensity, but it also successfully predicts the parabolic TEC cooling as a function of input voltage<sup>41</sup> due to coupled Joule and Peltier effect.

To demonstrate the multi-hotspot scenarios, Fig. 7 illustrates four prediction examples of a  $6 \times 6$  TEC array with the following: (a) random hotspots, (b) random hotspots + TEC cooling, (c) clustered hotspots and (d) clustered hotspots + TEC cooling. In the first two scenarios, nine arbitrary hotspots are assigned at random levels to represent a system incorporating

(a) Random hotspots ( $N_{HS}=9, N_{TEC}=0, m=n=6$ )

0	0	0	0	0	8	0	0	0	0	0	0	105	131	132	135	164	308	105	131	131	134	164	307	0.36	0.55	0.62	0.72	0.28	0.71
0	1	0	0	0	0	0	0	0	0	0	0	150	238	203	183	177	165	150	238	203	183	177	163	0.51	0.56	0.14	0.48	0.18	1.88
2	3	0	0	0	0	0	0	0	0	0	0	222	338	257	216	189	139	222	339	257	215	190	139	0.24	0.49	0.68	1.08	0.12	0.32
0	0	1	0	0	1	0	0	0	0	0	0	159	248	275	233	226	140	159	248	275	233	226	140	0.47	0.47	0.10	0.56	0.37	0.32
0	1	0	0	0	0	0	0	0	0	0	0	134	221	229	216	214	137	133	221	230	217	214	136	0.74	0.08	1.45	0.34	0.15	1.58
0	0	2	0	5	0	0	0	0	0	0	0	105	144	204	180	280	133	104	142	203	179	280	132	0.91	1.72	1.05	0.70	0.22	0.57

MAE =0.603

(b) Random hotspots + TEC cooling ( $N_{HS}=9, N_{TEC}=9, m=n=6$ )

0	0	0	0	0	8	0	0	0	0	0	4	150	149	161	169	170	84	150	148	161	168	169	84	0.42	1.19	0.02	0.23	0.99	0.80
0	1	0	0	0	0	0	0	3	0	0	0	137	87	148	157	159	170	138	83	145	158	160	169	0.82	4.05	2.85	0.62	1.40	0.31
2	3	0	0	0	0	0	0	4	1	0	0	46	201	170	149	135	165	48	198	170	149	136	168	1.61	2.95	0.21	0.18	1.23	3.39
0	0	1	0	0	1	0	0	0	0	1	4	154	175	185	133	52	151	155	176	186	131	51	155	0.99	0.53	1.55	1.36	0.97	3.97
0	1	0	0	0	0	0	0	0	0	1	0	157	159	149	137	117	155	158	158	152	139	118	159	0.78	0.55	2.94	2.39	1.62	3.28
0	0	2	0	5	0	0	0	0	0	2	0	149	151	110	147	95	157	151	150	109	148	94	161	2.00	1.07	0.72	0.50	1.66	3.55

MAE =1.491

(c) Clustered hotspots ( $N_{HS}=9, N_{TEC}=0, m=n=6$ )

0	0	0	0	0	0	0	0	0	0	0	0	114	171	195	181	136	95	114	171	193	180	133	92	0.49	0.71	1.16	1.49	2.84	2.34
0	2	2	2	0	0	0	0	0	0	0	0	171	365	430	390	230	124	171	363	428	389	229	122	0.39	2.28	1.56	0.98	0.87	1.48
0	2	2	2	0	0	0	0	0	0	0	0	195	430	511	462	271	137	194	428	509	461	270	137	0.60	1.50	2.23	1.67	0.91	0.55
0	2	2	2	0	0	0	0	0	0	0	0	181	390	462	421	251	131	180	389	461	420	251	131	0.54	1.54	1.27	1.01	0.25	0.15
0	0	0	0	0	0	0	0	0	0	0	0	136	230	271	251	181	109	134	228	268	250	180	108	2.16	2.43	2.22	1.05	0.93	1.06
0	0	0	0	0	0	0	0	0	0	0	0	95	124	137	131	109	84	93	122	135	130	108	83	2.13	1.68	1.79	1.10	1.19	0.82

MAE =1.315

(d) Clustered hotspots + TEC cooling ( $N_{HS}=9, N_{TEC}=9, m=n=6$ )

0	0	0	0	0	0	0	0	0	0	0	0	128	137	143	138	129	114	128	134	143	139	128	115	0.27	2.46	0.12	0.32	1.43	1.60
0	2	2	2	0	0	0	0	0	0	3	3	137	92	108	96	134	122	134	88	108	97	133	123	2.65	4.11	0.02	0.48	1.06	1.31
0	2	2	2	0	0	0	0	0	0	3	3	143	108	126	113	138	125	141	107	130	115	139	128	2.17	0.56	3.58	1.49	0.78	2.91
0	2	2	2	0	0	0	0	0	0	3	3	138	96	113	102	135	122	137	94	114	101	137	126	1.42	2.55	0.67	0.40	1.80	4.00
0	0	0	0	0	0	0	0	0	0	0	0	129	134	138	135	130	115	128	134	140	137	133	118	1.19	0.01	1.50	2.20	2.88	3.52
0	0	0	0	0	0	0	0	0	0	0	0	114	122	125	122	115	103	114	123	127	124	117	107	0.49	1.28	1.42	1.07	2.65	3.52

MAE =1.664

Hotspot input

TEC input

Ground truth

CNN prediction

Local error

FIG. 7. Case studies of a  $6 \times 6$  array for temperature prediction (unit:  $^{\circ}\text{C}$ ). (a) Arbitrary hotspots without TECs. (b) Arbitrary hotspots with TECs (not optimal). (c) Clustered hotspots without TECs. (d) Clustered hotspots with TECs (not optimal).

different modules that may experience various local heating conditions. In the last two scenarios, on the other hand, nine assigned hotspots are clustered within a  $3 \times 3$  region with equal intensity to mimic a system consisting of similar components that undergo simultaneous workloads. It is observed that the orderly and clustered scenarios exhibit slightly higher MAE loss compared to the scattered and random scenarios due to the lower likelihood of generating well-organized data during data generation. Furthermore, for Fig. 7b and 7d, larger MAE loss is identified owing to the introduction of TEC cooling mechanism. Nevertheless, the key features of the TEC array can be safely captured: First of all, significant lateral heat redistribution can be observed from the predictions, where higher temperature occurs near the TEC-assigned regions compared to their hotspots-only counterparts. Secondly, the clustered TECs are predicted to have poorer effectiveness compared to the isolated TECs with

the same intensity. This is because the adjacent TECs tend to generate active heat flow against each other, resulting in inefficient cooling. Lastly, local TEC cooling can be influenced by its corresponding hotspot conditions. A TEC is more likely to provide greater temperature reduction when its local hotspot has higher intensity. In summary, local TEC cooling will impact and be impacted by the surrounding TECs and hotspots. Therefore, achieving a global optimal solution is almost impossible by simply considering the local optimal TEC control.

#### IV. TEC OPTIMIZATION ALGORITHM

Due to the complex dependency among TEC array and multiple hotspots, using the traditional FEM-based techniques to enumerate all possible solutions seem difficult and even impossible. However, with efficient optimization algorithm based on machine learning model, real-time global optimal solution can be feasible. In this study, we set our target to find the global optimal temperature (i.e., the smallest peak temperature) based on the existing hotspot conditions, while other possibilities, such as looking for the minimum TEC power/TEC counts for achieving acceptance temperature, can also be possible. Fig. 8

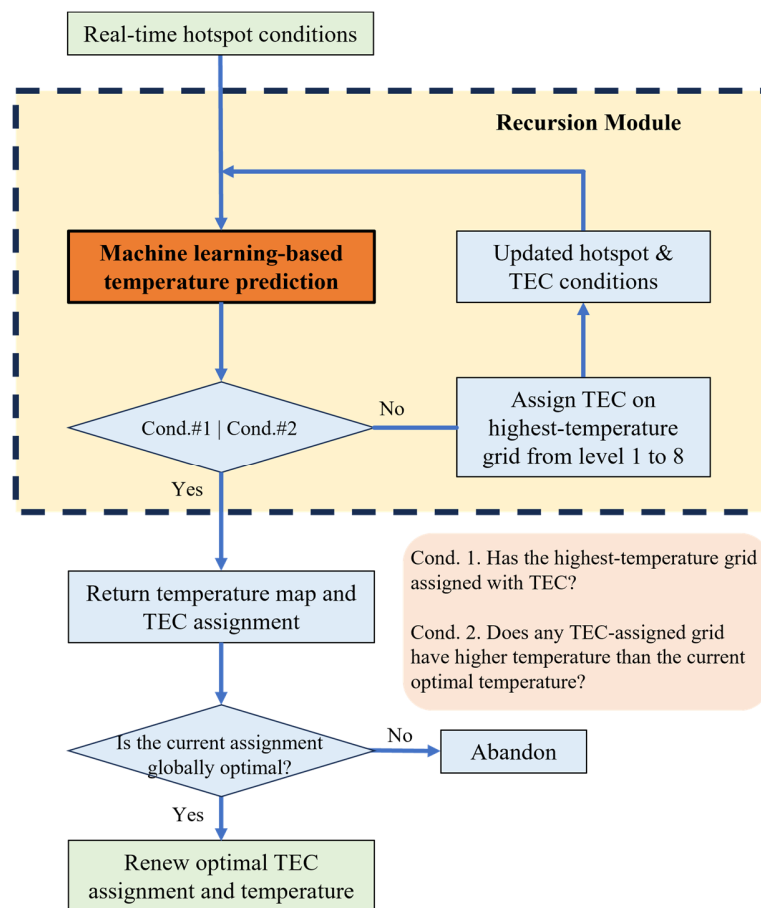


FIG. 8. Flowchart of backtracking-based TEC decision-making algorithm.

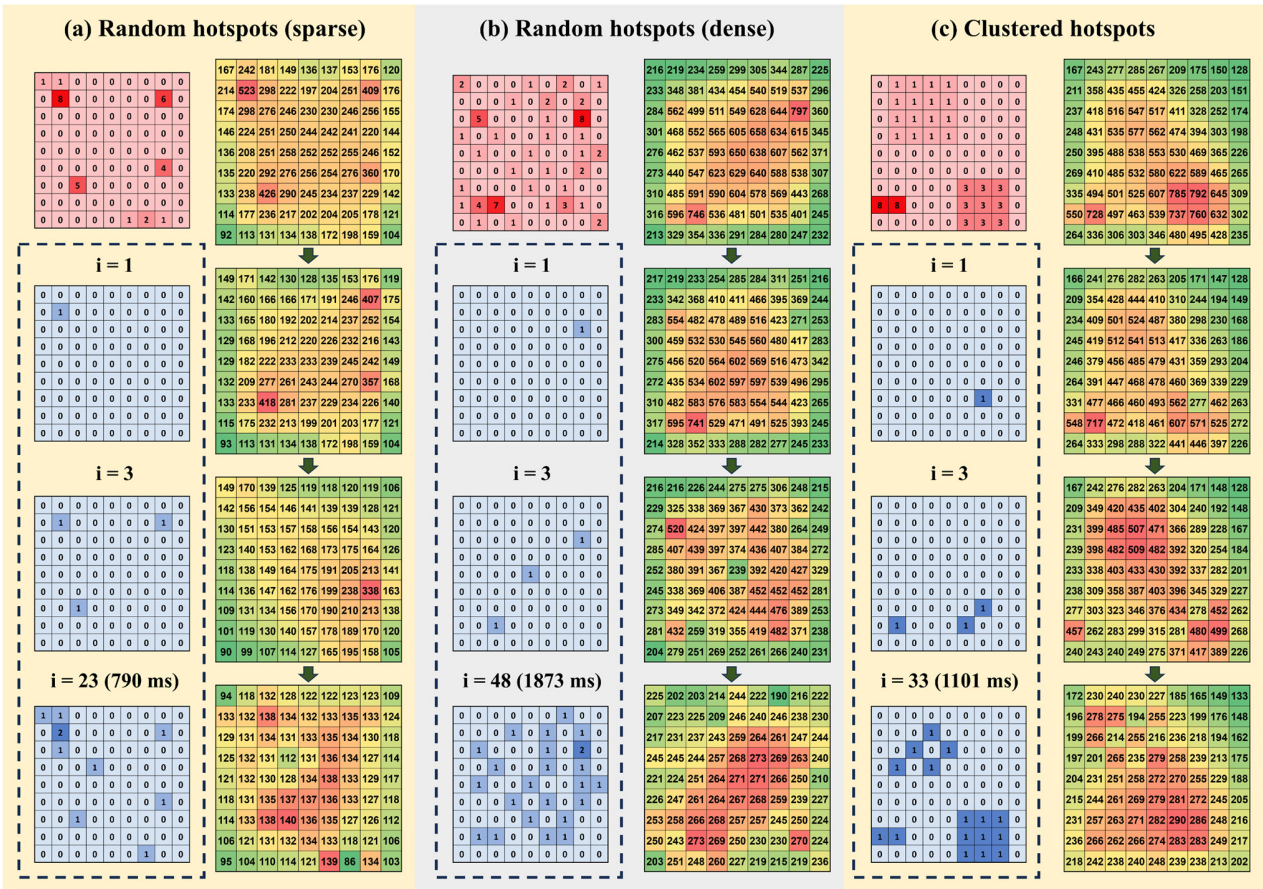


FIG. 9. Case studies of a  $9 \times 9$  array for backtracking-based decision-making (unit:  $^{\circ}\text{C}$ ). The pink matrix represents the real-time hotspot conditions, the blue matrix represents the current optimal TEC assignments within  $i$  iterations and the red-green matrix denotes the predicted global optimal temperature map. The last row of each case represents their final optimal solutions. Three scenarios are discussed: (a) Random sparse hotspots. (b) Random dense hotspots. (c) Clustered hotspots.

demonstrates the flowchart of the backtracking-based<sup>43,44</sup> TEC decision-making algorithm. The established CNN model was used as a function to efficiently evaluate the current status. Based on the specific problem, two assumptions were made: first, the highest-temperature grid has the most priority to assign the TEC. Second, once a grid is assigned with TEC, its temperature will always increase by any further TEC assignment next to it. Only when these two assumptions hold will the algorithm look for a deeper solution based on the existing ones. Fig. 9 demonstrates three cases of the  $9 \times 9$  TEC array control using the developed algorithm: (a) Random sparse hotspots. (b) Random dense hotspots. (c) Clustered hotspots. The highest temperatures of three samples (i.e.,  $523^{\circ}\text{C}$ ,  $797^{\circ}\text{C}$ ,  $792^{\circ}\text{C}$ , respectively) experience substantial temperature reduction (i.e., dropped down to  $140^{\circ}\text{C}$ ,  $273^{\circ}\text{C}$  and  $290^{\circ}\text{C}$ , respectively) after optimal TEC control. The total iteration counts (and times) are 23 (790ms), 48 (1873ms) and 33 (1101ms), respectively. All samples show a trend of the hotspot migrating towards the center as the optimization process evolves. This is because the process of finding the global optimal temperature inherently drives the system towards a more uniform temperature field, which manifests as a decreasing global temperature gradient due to TEC heat

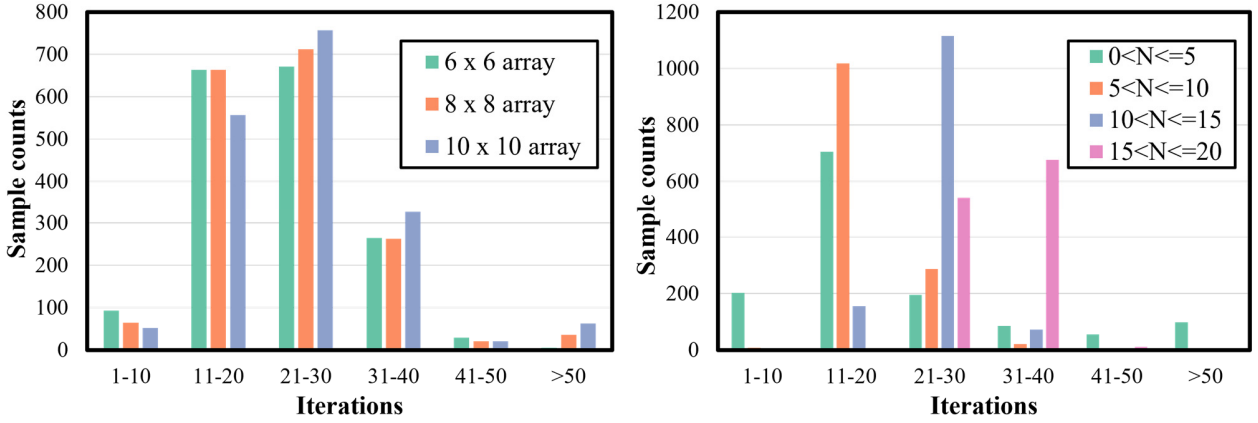


FIG. 10. Efficiency analysis of 6000 random samples using machine learning-assisted TEC optimization algorithm. (a) Iteration statistics of various array dimensions. (b) Iteration statistics of various hotspot counts.

TABLE. II. Summary of single prediction time between simulation and CNN model

$m \times n$	Test samples	Maximum simulation time	Minimum simulation time	Average simulation time	Average CNN prediction time
[1,25]	1530	34s	4s	19s	41ms
[26,50]	900	83s	30s	53s	43ms
[51,75]	390	112s	73s	91s	42ms
[76,100]	180	168s	106s	128s	42ms

TABLE. III. Summary of running time for machine learning-assisted TEC optimization

Number of hotspots	Test samples	Maximum time (iterations)	Minimum time (iterations)	Average time (iterations)
[1,5]	1500	98.73s (2323)	0.24s (5)	1.17s (27)
[6,10]	1500	2.54s (60)	0.33s (7)	0.77s (18)
[11,15]	1500	2.39s (59)	0.46s (13)	1.04s (24)
[16,20]	1500	2.98s (72)	0.78s (18)	1.30s (31)

redistribution. It is worth noting that only small intensities of TEC (i.e., 1 or 2) are found in the optimal TEC assignments, while those large intensities of TEC may either cause too much penalty (i.e., temperature rise) to its neighboring or generate too much local Joule heat, which are abandoned by the optimization algorithm. This again demonstrates the fact that a local optimal TEC control may not suffice for the global optimal temperature.

Fig. 10 demonstrates the efficiency analysis based on 6000 samples using machine learning-assisted TEC optimization algorithm. A total of 2000 samples are generated for each array size of  $6 \times 6$ ,  $8 \times 8$  and  $10 \times 10$ . For each array size, 10 samples are randomly generated with given  $N_{HS}$  from 1 to 20. It is observed that the iteration counts predominantly fall within the range of [21,30], with an average value of 25. In general, a large array size and a large  $N_{HS}$  can lead to more iteration counts due to more enumerable TEC control options. However, it is possible to encounter unacceptably high iteration counts when dealing

with too small  $N_{HS}$  values (i.e.,  $1 \leq N_{HS} \leq 2$ ). This is because a very small  $N_{HS}$  combined with a large array ( $10 \times 10$ ) can easily lead to nearly zero temperature gradient after TEC assignments. Additional constraints can be defined to address this issue, such as setting maximum iteration counts and acceptance temperatures.

To further investigate the efficiency of the machine learning-based TEC optimization algorithm, we record the single prediction time in Table. II for both FEM simulation and CNN model within 3000 samples as mentioned in Fig. 5. Following this, in Table. III, we summarize the running time for the optimization algorithm using the 6000 samples mentioned in Fig. 10. All FEM simulations are performed using COMSOL 6.0 with CPU computation on an AMD Ryzen 9 3950X processor (16-core, 3.5GHz) and 128GB memory, with a maximum of 1,582,714 degrees of freedom. The CNN model predictions are computed using GPU acceleration on a NVIDIA GeForce RTX 2080Ti (11GB) with a total of 84,475,804 parameters. Based on the statistical results, the average FEM simulation time for a single prediction is found to be 45s. Larger array sizes generally result in a longer computational time due to the increased degrees of freedom. Conversely, the CNN prediction demonstrates similar computational cost through various input variables with an averaging prediction time of only 42ms. A speed increase in an order of  $10^3$  is found when using the CNN model to conduct a single temperature prediction compared to the traditional FEM methods. Furthermore, with the acceleration of the CNN model, the TEC optimization algorithm can be carried out within an average time of 1.07s, where the same amount of FEM computation will take about 18 minutes, representing a significant speed-up of 26000 times.

## V. CONCLUSIONS

In this study, we present a novel machine learning-assisted TEC optimization algorithm aimed at achieving global optimal temperature control for on-demand multi-hotspot thermal management in microelectronic systems. Our findings demonstrate the ability of the machine learning-assisted algorithm to dynamically adapt to the evolving thermal landscape of microelectronic devices, efficiently offering optimal TEC control for managing the spatial and temporal variations of hotspots. The algorithm not only mitigates the computational burdens associated with the traditional FEM-based optimization techniques but also heralds a significant leap towards achieving the on-demand thermal management imperative for the sustainability and performance of advanced semiconductor devices.

## CONFLICT OF INTEREST

The authors have no conflicts to disclose.

## DATA AVAILABILITY

The data that support the findings of this study are available from the corresponding author upon reasonable request.

## REFERENCES

- <sup>1</sup> Samsung Newsroom, “Samsung Begins Chip Production Using 3nm Process Technology With GAA Architecture,” <https://News.Samsung.Com/Global/Samsung-Begins-Chip-Production-Using-3nm-Process-Technology-with-Gaa-Architecture>, (2022).
- <sup>2</sup> R. Saleh, S. Wilton, S. Mirabbasi, A. Hu, M. Greenstreet, G. Lemieux, P.P. Pande, C. Grecu, and A. Ivanov, “System-on-chip: Reuse and integration,” *Proceedings of the IEEE* 94(6), 1050–1068 (2006).
- <sup>3</sup> W. Wolf, A.A. Jerraya, and G. Martin, “Multiprocessor system-on-chip (MPSoC) technology,” *IEEE Transactions on Computer-Aided Design of Integrated Circuits and Systems* 27(10), 1701–1713 (2008).
- <sup>4</sup> J.M.P. Cardoso, K.C. Morrow, P.C. Diniz, and Institute of Electrical and Electronics Engineers, in (n.d.).
- <sup>5</sup> M.R. Stan, K. Skadron, M. Barcella, W. Huang, K. Sankaranarayanan, and S. Velusamy, in *Microelectronics J* (Elsevier Ltd, 2003), pp. 1153–1165.
- <sup>6</sup> A. Gupte, and P. Jones, in *ReConFig’09 - 2009 International Conference on ReConFigurable Computing and FPGAs* (2009), pp. 89–94.
- <sup>7</sup> K.C.J. Chen, C.H. Chao, and A.Y.A. Wu, “Thermal-Aware 3D Network-On-Chip (3D NoC) Designs: Routing Algorithms and Thermal Managements,” *IEEE Circuits and Systems Magazine* 15(4), 45–69 (2015).
- <sup>8</sup> M. Engel, M. Steiner, J.W.T. Seo, M.C. Hersam, and P. Avouris, “Hot spot dynamics in carbon nanotube array devices,” *Nano Lett* 15(3), 2127–2131 (2015).
- <sup>9</sup> C.J.M. Lasance, “Thermally driven reliability issues in microelectronic systems: Status-quo and challenges,” *Microelectronics Reliability* 43(12), 1969–1974 (2003).
- <sup>10</sup> Y. Yu, W. Zhu, X. Kong, Y. Wang, P. Zhu, and Y. Deng, “Recent development and application of thin-film thermoelectric cooler,” *Front Chem Sci Eng* 14(4), 492–503 (2020).
- <sup>11</sup> T. Guclu, and E. Cuce, “Thermoelectric Coolers (TECs): From Theory to Practice,” *J Electron Mater* 48(1), 211–230 (2019).
- <sup>12</sup> W.Y. Chen, X.L. Shi, J. Zou, and Z.G. Chen, “Thermoelectric coolers for on-chip thermal management: Materials, design, and optimization,” *Materials Science and Engineering R: Reports* 151, (2022).
- <sup>13</sup> G. Bulman, P. Barletta, J. Lewis, N. Baldasaro, M. Manno, A. Bar-Cohen, and B. Yang, “Superlattice-based thin-film thermoelectric modules with high cooling fluxes,” *Nat Commun* 7, (2016).
- <sup>14</sup> I. Chowdhury, R. Prasher, K. Lofgreen, G. Chrysler, S. Narasimhan, R. Mahajan, D. Koester, R. Alley, and R. Venkatasubramanian, “On-chip cooling by superlattice-based thin-film thermoelectrics,” *Nat Nanotechnol* 4(4), 235–238 (2009).
- <sup>15</sup> Z. Ren, and J. Lee, “Thermal conductivity anisotropy in holey silicon nanostructures and its impact on thermoelectric cooling,” *Nanotechnology* 29(4), (2018).
- <sup>16</sup> Z. Ren, J. Cao, J. Lim, Z. Yu, J.C. Kim, and J. Lee, “Experimental Demonstration of Holey Silicon-Based Thermoelectric Cooling,” *IEEE Trans Electron Devices* 69(6), 3446–3454 (2022).
- <sup>17</sup> O. Sullivan, M.P. Gupta, S. Mukhopadhyay, and S. Kumar, “Array of thermoelectric coolers for on-chip thermal management,” *Journal of Electronic Packaging, Transactions of the ASME* 134(2), (2012).
- <sup>18</sup> L.M. Goncalves, J.G. Rocha, C. Couto, P. Alpuim, and J.H. Correia, “On-chip array of thermoelectric Peltier microcoolers,” *Sens Actuators A Phys* 145–146(1–2), 75–80 (2008).
- <sup>19</sup> H. Kattan, S.W. Chung, J. Henkel, and H. Amrouch, “On-Demand Mobile CPU Cooling with Thin-Film Thermoelectric Array,” *IEEE Micro* 41(4), 67–73 (2021).
- <sup>20</sup> H. Fateh, C.A. Baker, M.J. Hall, and L. Shi, “High fidelity finite difference model for exploring multi-parameter thermoelectric generator design space,” *Appl Energy* 129, 373–383 (2014).
- <sup>21</sup> T. Wang, C. Zhang, H. Snoussi, and G. Zhang, “Machine Learning Approaches for Thermoelectric Materials Research,” *Adv Funct Mater* 30(5), (2020).

- <sup>22</sup> L. Chen, W. Jin, J. Zhang, and S.X.D. Tan, “Thermoelectric Cooler Modeling and Optimization via Surrogate Modeling Using Implicit Physics-Constrained Neural Networks,” *IEEE Transactions on Computer-Aided Design of Integrated Circuits and Systems* 42(11), 4090–4101 (2023).
- <sup>23</sup> P. Zhang, D.W. Wang, W.S. Zhao, B. You, J. Liu, C. Qian, and H.B. Xu, “Intelligent Design and Tuning Method for Embedded Thermoelectric Cooler (TEC) in 3-D Integrated Microsystems,” *IEEE Trans Compon Packaging Manuf Technol* 13(6), 788–797 (2023).
- <sup>24</sup> J. Zhang, S. Sadiqbatcha, L. Chen, C. Thi, S. Sachdeva, H. Amrouch, and S.X.D. Tan, “Hot-spot aware thermoelectric array based cooling for multicore processors,” *Integration* 89, 73–82 (2023).
- <sup>25</sup> J. Luo, J. Lim, J. Chen, A. Venugopal, Z. Ren, and J. Lee, “Dynamic Thermal Management in SOI Transistors Using Holey Silicon-Based Thermoelectric Cooling,” *IEEE Trans Electron Devices*, 1–8 (2024).
- <sup>26</sup> J. Lee, J. Lim, and P. Yang, “Ballistic phonon transport in holey silicon,” *Nano Lett* 15(5), 3273–3279 (2015).
- <sup>27</sup> J. Tang, H.T. Wang, D.H. Lee, M. Fardy, Z. Huo, T.P. Russell, and P. Yang, “Holey silicon as an efficient thermoelectric material,” *Nano Lett* 10(10), 4279–4283 (2010).
- <sup>28</sup> N. Liu, T. Zhu, M.G. Rosul, J. Peters, J.E. Bowers, and M. Zebarjadi, “Thermoelectric properties of holey silicon at elevated temperatures,” *Materials Today Physics* 14, (2020).
- <sup>29</sup> J. Ma, D. Gelda, K. V. Valavala, and S. Sinha, “Peak thermoelectric power factor of holey silicon films,” *J Appl Phys* 128(11), (2020).
- <sup>30</sup> J. Schmidhuber, “Deep Learning in neural networks: An overview,” *Neural Networks* 61, 85–117 (2015).
- <sup>31</sup> Y. Lecun, E. Bottou, Y. Bengio, and P. Haffner, *Gradient-Based Learning Applied to Document Recognition* (1998).
- <sup>32</sup> K. Simonyan, and A. Zisserman, “Very Deep Convolutional Networks for Large-Scale Image Recognition,” (2014).
- <sup>33</sup> C. Szegedy, W. Liu, Y. Jia, P. Sermanet, S. Reed, D. Anguelov, D. Erhan, V. Vanhoucke, and A. Rabinovich, *Going Deeper with Convolutions* (n.d.).
- <sup>34</sup> C. Szegedy, V. Vanhoucke, S. Ioffe, and J. Shlens, *Rethinking the Inception Architecture for Computer Vision* (n.d.).
- <sup>35</sup> A. Li, R. Chen, A.B. Farimani, and Y.J. Zhang, “Reaction diffusion system prediction based on convolutional neural network,” *Sci Rep* 10(1), (2020).
- <sup>36</sup> C. Rao, P. Ren, Q. Wang, O. Buyukozturk, H. Sun, and Y. Liu, “Encoding physics to learn reaction–diffusion processes,” *Nat Mach Intell* 5(7), 765–779 (2023).
- <sup>37</sup> W. Jin, W. Zhang, J. Hu, B. Weng, T. Huang, and J. Chen, “Using the Residual Network Module to Correct the Sub-Seasonal High Temperature Forecast,” *Front Earth Sci (Lausanne)* 9, (2022).
- <sup>38</sup> V. Nair, and G.E. Hinton, *Rectified Linear Units Improve Restricted Boltzmann Machines* (n.d.).
- <sup>39</sup> M. Lin, Q. Chen, and S. Yan, “Network In Network,” (2013).
- <sup>40</sup> Z. Wang, and A.C. Bovik, “Mean squared error: Lot it or leave it? A new look at signal fidelity measures,” *IEEE Signal Process Mag* 26(1), 98–117 (2009).
- <sup>41</sup> J.E. Parrott, *THE INTERPRETATION OF THE STATIONARY AND TRANSIENT BEHAVIOUR OF REFRIGERATING THERMOCOUPLES* (1960).
- <sup>42</sup> A. Ghosh, H. Kumar, and P.S. Sastry, “Robust Loss Functions under Label Noise for Deep Neural Networks,” *Proceedings of the AAAI Conference on Artificial Intelligence* 31(1), (2017).
- <sup>43</sup> P. van Beek, in (2006), pp. 85–134.
- <sup>44</sup> P. Civicioglu, “Backtracking Search Optimization Algorithm for numerical optimization problems,” *Appl Math Comput* 219(15), 8121–8144 (2013).